Article

Operando Local pH Measurement within Gas Diffusion Electrodes Performing Electrochemical Carbon Dioxide Reduction

Alex J. Welch, Aidan Q. Fenwick, Annette Böhme, Hsiang-Yun Chen, Ian Sullivan, Xueqian Li, Joseph S. DuChene, Chengxiang Xiang, and Harry A. Atwater*

Read Online

ACCESS | Metrics & More | Article Recommendations | Supporting Information

ABSTRACT: The local pH near the surface of a CO_2 reduction electrocatalyst strongly impacts catalytic selectivity and activity. Here, confocal fluorescence microscopy was used to map the electrolyte pH near a copper gas diffusion electrode during CO_2 reduction with micron spatial resolution in three dimensions. We observed that the local pH increased from pH 6.8 to greater than pH 10 as the current density was increased from 0 to 28 mA/cm² in a 100 mM $KHCO_3$ electrolyte. Variations in the pH across the surface indicate areas of locally increased activity. Within deep trenches of the active layer, the local pH increases as trench width decreases. Computational models confirm these experimental results and also showed that the catalyst found within narrow trenches is more active than that found at the surface of the electrode. This study suggests that the overpotential required to perform selective CO_2 reduction can be reduced by increasing the density of narrow trench regions in the microporous layer.
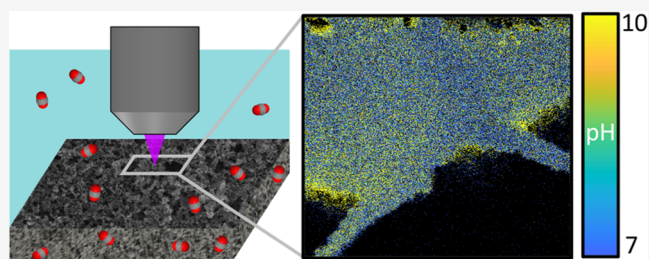
INTRODUCTION

While the cost of renewable electricity has declined markedly, selective, energy-efficient synthesis of storable chemical fuels is necessary to enable widespread adoption of sustainable energy. One approach is to transform solar energy into chemical fuels and fuel precursors via artificial photosynthesis. Recently, significant advances have been made in the design of gas diffusion electrodes (GDEs) for electrochemical carbon dioxide (CO_2) reduction at high current densities. While promising, GDEs have not yet achieved their full potential for product selectivity and energy efficiency due to the complexity of the electrocatalytic reactions involved in making fuels from CO_2 reduction.

Many parameters may influence the selectivity and activity of the CO_2 reduction reaction, the most obvious of which are the catalyst[1−3] and applied potential.[4,5] Aside from these two critical parameters, GDE system configurations (flow through vs. flow by),[6] local electrolyte viscosity,[7] concentration and identity of cations in the electrolyte,[8] salt deposition on the GDE,[9] membrane structure and composition,[10] bicarbonate and carbonate formation in the electrolyte,[11] hydrophobicity of the GDE,[12] and other factors can have a significant influence on device performance.

Of particular interest in this work is the local pH established at the electrode surface during fuel synthesis. Electrochemical solar fuel-forming reactions create hydroxide ions (OH^-) at the catalyst surface during the reaction when in alkaline electrolyte, which alters the local pH near the cathode,[13,14] thus strongly impacting both product selectivity and

activity.[15−18] Therefore, it is important to distinguish the local pH near the electrode surface from the pH in the bulk electrolyte. Although challenging to determine experimentally, the local pH near the electrode surface should be measured under operating conditions to provide the necessary insight required to further improve the activity, selectivity, and stability of these fuel-forming devices.

In this study, we focus on understanding the pH in GDEs because this device architecture has increased the performance of CO_2 reduction electrodes by an order of magnitude due to their ability to deliver CO_2 in the gas phase, thereby overcoming the mass transport limitations encountered in more traditional electrocatalytic devices.[19] Not only does this architecture allow for higher current densities, but also improved product selectivity in CO_2 reduction.[19−21] In CO_2 reduction devices where the CO_2 is dissolved directly into the electrolyte, the maximum current density is less than −30 mA/cm² due to low CO_2 solubility in aqueous electrolytes (around [34 mM] at maximum).[22] The main challenge of the GDE architecture is in developing the appropriate device structure to maintain what is referred to as a "wetted" condition. Here, a thin layer of electrolyte coats the catalyst to provide water
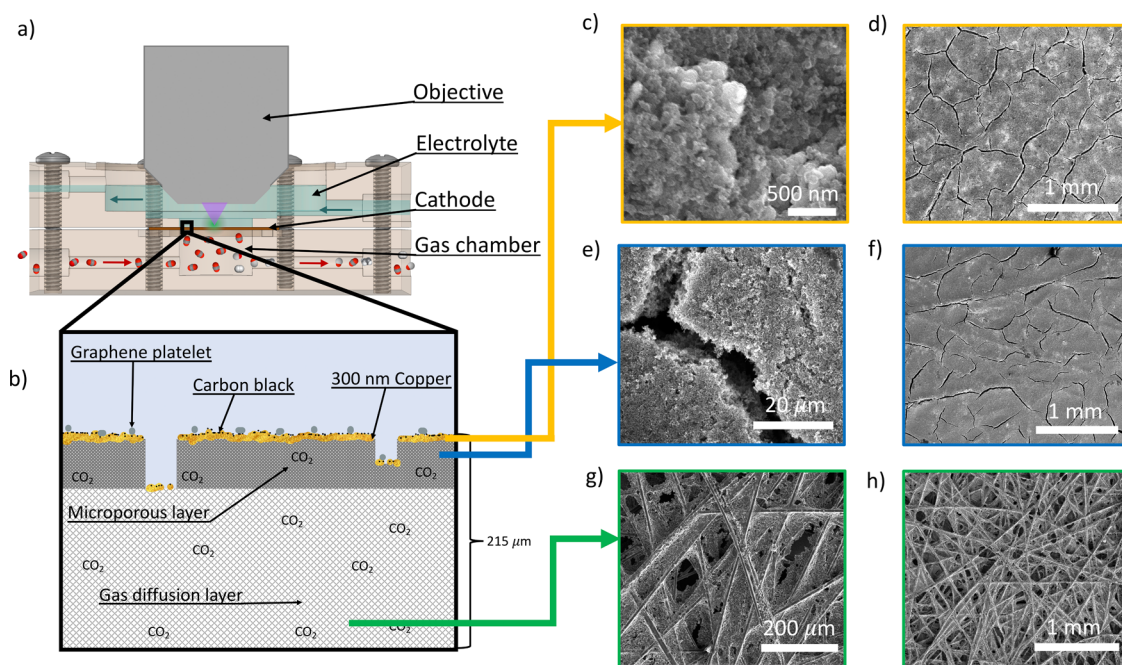
Figure 1. Overview of a Cu gas diffusion electrode (GDE) for CO_2 reduction studies. (a) Cross-sectional diagram of the custom electrochemical cell designed to enable in situ confocal fluorescence microscopy experiments. (b) Schematic of a typical Cu GDE, not to scale. (c, d) Scanning electron microscopy (SEM) images of the 300 nm thick Cu catalyst layer. (e, f) SEM images of an uncoated microporous layer. (g, h) SEM images of the gas diffusion layer.

molecules while simultaneously allowing for rapid dissolution of CO_2 through the electrolyte to avoid mass transport limitations. If the water layer coating the catalyst is too thick, then the catalyst becomes flooded and its operation is more similar to a bulk aqueous electrolyte CO_2 reduction device.[23] Alternatively, if there is no electrolyte, the catalyst has no access to water molecules and no reaction can occur. To achieve this wetted condition, the GDE is composed of a gas diffusion layer, microporous layer, and catalyst layer (Figure 1). The microporous layer is perhaps the most critical because the concentration of poly(tetrafluoroethylene) (PTFE) allows the wetting to be tuned.[12,23] Tailored GDE architectures have demonstrated current densities greater than 1 A/cm^2 for multicarbon products.[24]

It is vital to understand the local pH within GDEs due to the high CO_2 flow rates and high current densities at which these devices operate. Interestingly, these two characteristics have opposing effects on the local pH near the electrode surface. High current densities result in the creation of multiple hydroxide ions per unit time, thus rapidly increasing the pH, while any unreacted CO_2 will acidify the electrolyte via reaction with OH^- to form HCO_3^- and H^+ ions. If the pH is increased locally, then the activity of the hydrogen evolution reaction (HER) decreases substantially, while the CO_2 reduction reaction becomes relatively more favorable.[17,18] While both reactions consume water molecules, the rate of H_2 evolution has been shown to be far more dependent on the local pH than the rate of CO_2 reduction.[17,25] In addition to suppressing the HER, the local pH also influences which CO_2 reduction pathways are most energetically favorable.[16,18,26] Alkaline conditions in particular promote the formation of multicarbon products (C_{2+}) such as ethanol, propanol, acetate, etc.[16,25,26] Theoretical models have been developed to simulate the local pH near operating CO_2 reduction GDEs;[23,27,28] however, it is difficult to accurately represent the complex

electrochemical environment created by the triple phase boundary at the catalyst surface. We therefore seek to directly measure the local pH near an operating GDE and experimentally validate the results of these prior simulations.

There are various techniques that can be used to probe the local pH, such as fluorescence microscopy,[15,29−34] scanning electrochemical cell microscopy (SECM),[35−37] surface-enhanced Raman spectroscopy (SERS),[38] and surface-enhanced infrared absorption spectroscopy (SEIRAS).[39] Previously, SERS has been used to measure the local pH in a CO_2 reduction GDE with a 1 M KOH electrolyte (pH 14). It was found that the local pH was near 7 in the absence of any current flow, and as the current density increased to 100 mA/cm^2, the local pH increased to 10. It is interesting to note that even with an electrolyte with a bulk pH of 14, the electrode surface remained in the range pH range of 7−10 for a wide range of current densities. However, this measurement did not provide any resolution along the plane of the electrode surface. SECM studies confirm that the local pH increases during device operation.[35−37] While SECM allows for better spatial resolution than confocal fluorescence microscopy, it is unable to probe the pH within the trenches of the GDE (Figure 1e,f). Our study builds on previous work by mapping the pH both on the surface and within the heterogeneous reaction environments encountered in GDEs. This experimental approach therefore allows us to correlate the width of trenches in GDEs to the local pH.

Here, we use confocal microscopy and a pH-sensitive two-color fluorescent dye to probe the *operando* local pH of a copper (Cu) GDE under CO_2 reduction conditions with micron-scale resolution in all three spatial dimensions [within the plane of the electrode (x, y) and perpendicular to its surface (z)]. This approach offers new insight into how CO_2 reduction affects the local electrolyte pH near the Cu catalyst. Interestingly, our study indicates that at low overpotentials, the
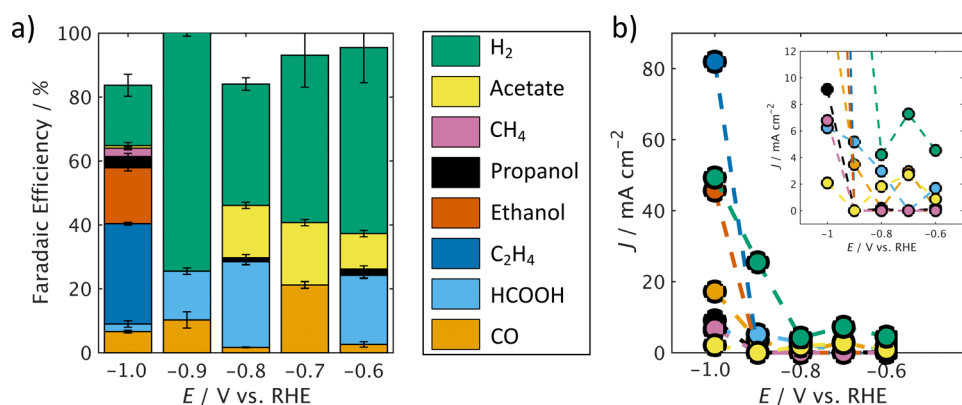
Figure 2. Electrocatalytic characterization of a GDE composed of carbon paper coated with 300 nm of Cu on top of the microporous layer. (a) Faradaic efficiency and (b) partial current density, J, for each product as a function of electrode potential, E. The figure legend applies to both panels (a) and (b).

pH varies widely across the electrode surface. Specifically, in narrow trenches throughout the electrode, the pH is significantly elevated compared to the surroundings. Our findings highlight the electrocatalytic heterogeneity in GDEs and strongly suggest that these regions of locally high pH are the most active parts of the electrode for CO_2 reduction.

A Cu-based GDE was investigated owing to the unique ability of Cu to produce C_{2+} products (e.g., ethanol).[3,40] Figure 1 shows a schematic of the GDE and experimental setup used, as well as scanning electron microscopy (SEM) and optical bright-field microscopy images of different layers of the device. The GDE used here and in many other devices[19,25,41,42] is composed of three layers: (1) a gas diffusion layer, (2) a microporous layer, and (3) a catalyst layer (Figure 1b). The CO_2 first diffuses through the gas diffusion layer, composed of carbon fibers (Figure 1g,h), and then through the microporous layer, which is made of carbon black coated in hydrophobic PTFE to regulate local electrolyte availability (Figure 1e,f). After diffusion through the microporous layer, CO_2 comes into contact with the electrolyte at the catalyst layer (Figure 1c,d), where it can then undergo reduction to yield a variety of chemical products.

Some CO_2 reacts at the catalyst surface into products such as CO, HCOOH, or CH_4. The remaining unreacted portion of the CO_2 then passes into the electrolyte and increases its acidity.[43] While several reports quantified the one pass CO_2 utilization efficiency,[44] the vast majority of the CO_2 reduction experiments did not seek to optimize the utilization of CO_2. The competition between these two processes—CO_2 acidification and hydroxide ion generation—can be investigated via measurement of the local pH at the catalyst−electrolyte interface.

METHODS

We used confocal fluorescence microscopy to measure the local pH due to its high spatial resolution relative to the dimensions of interest in the system. Figure 1a shows a schematic of the experimental setup, and Figure S1 shows a more detailed schematic, as well as photos of the cell. The technical resolution of this system is 280 nm in $x − y$ and 560 nm in z. However, due to noise from the electrolyte pump and diffusion, the resolution is on the order of a micron under our conditions. A laser is used to excite a ratiometric two-color pH-sensitive fluorescent dye, 6,8-dihydroxy-1,3-pyrenedisulfonic acid (DHPDS) in the electrolyte.[45] This approach ensures that

the pH is independent of the concentration of DHPDS in the solution.[15] Figure S2 shows the absorbance vs wavelength of DHPDS in different standard solutions of known pH. At the most acidic pH of 4.6, the peak absorbance is centered at ∼400 nm; at pH 8.5, the peak absorbance is at ∼455 nm; and at pH 11.7, the peak absorbance shifts toward ∼480 nm. We focused our studies on near-neutral to basic pH conditions based on the results of previous work,[22,25] which reported that these conditions are most favorable for CO_2 reduction. We therefore sequentially excite the dye line by line with a 458 nm (λ_{ex1}) and 488 nm (λ_{ex2}) laser to achieve the resolution over the widest range of relevant pH values. The fluorescence signal from both λ_{ex1} and λ_{ex2} is collected individually from 515 to 700 nm. In Figure S2b, the ratio of the fluorescence intensity from λ_{ex1} and λ_{ex2} is plotted versus solution pH. These data demonstrate that the DHPDS dye is sensitive to changes in solution pH from pH 6 to 10 under the aforementioned excitation conditions. After fitting the calibration curve, we find that the error in pH is 0.3 pH units.

A CO_2-saturated solution of 100 mM $KHCO_3$ with a bulk pH of 6.8 was used as the electrolyte in our experiments, ensuring that the bulk pH will be at the lower-sensitivity limit of the DHPDS. The DHPDS dye is electrochemically stable under CO_2 reduction reaction conditions (Figures S2c and S3). In Figure S2c, the current−voltage characteristics of the electrode are nearly identical with or without the ratiometric dye. Upon addition of the dye, HER activity slightly increased but left the CO_2 reduction reaction activity remains largely unchanged (Figure S3). Based on these control experiments, the DHPDS dye is relatively inert with regard to GDE operating conditions.

RESULTS AND DISCUSSION

We first characterized the electrochemical performance of our Cu-based GDE prior to imaging the local solution pH. For details on electrode fabrication and cell setup, see the Methods section in the Supporting Information. Chronoamperometry experiments were performed across a range of applied potentials, and the products were measured via gas chromatography and high-performance liquid chromatography (Figure 2). All applied potentials (E) are reported vs the reversible hydrogen electrode (E vs RHE). As shown in Figure 2a, at potentials more positive than −1.0 V vs RHE, the Cu GDE produced primarily H_2 with some C_1 and C_2 products. Consistent with prior observations from Cu GDEs, H_2 is the
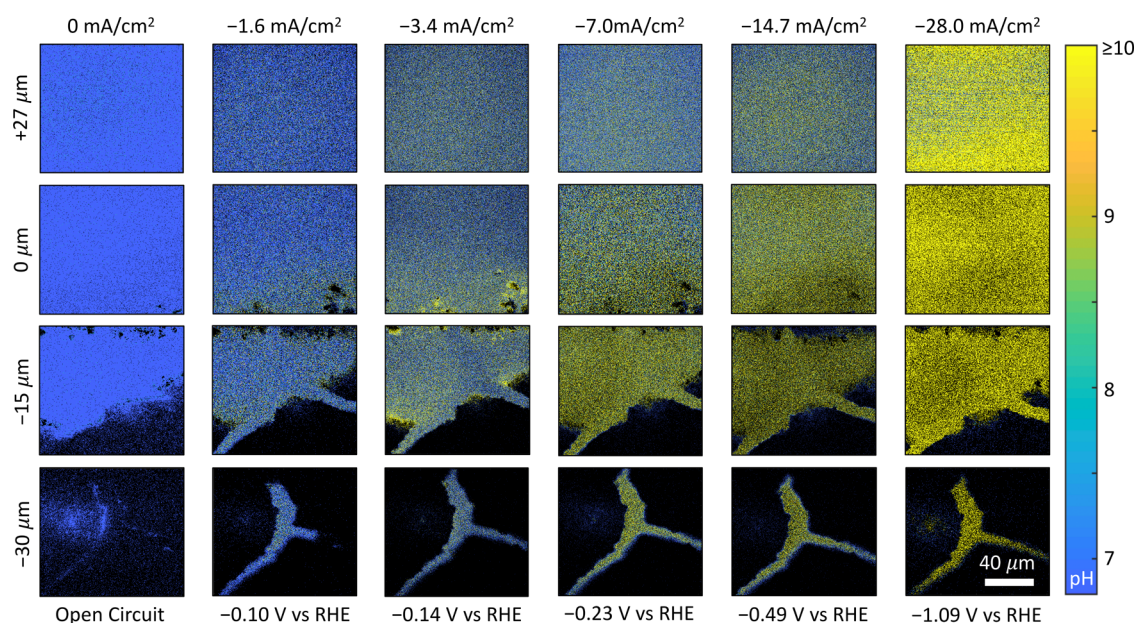
Figure 3. Operando mapping of solution pH in three dimensions over a Cu GDE. Maps are obtained at the same location on the electrode at different heights above the electrode surface and at different current densities. From top to bottom, each row of maps corresponds to 27 μm above, 0 μm (at the surface), 15 μm below, and 30 μm below the electrocatalyst surface. From left to right, each column of maps were obtained at 0 mA/cm^2 (no reaction under open-circuit conditions), −1.6, −3.4, −14.7, and −28.0 mA/cm^2. The pH color scale and the scale bar in the bottom right corner apply to all images.

dominant product at low overpotentials, while higher overpotentials favor CO_2 reduction.[4,46] Cu requires higher overpotentials to perform the C−C coupling reactions necessary to synthesize C_2 products.[21] At −1.0 V vs RHE, we begin to observe many CO_2 reduction products, with the largest fraction consisting of C_2 products, ethylene and ethanol. Higher overpotentials were not evaluated because the limited pH sensitivity range of the DHPDS dye is not suited for higher current densities. We therefore restricted our electrocatalytic characterization to those conditions that could be directly examined with confocal microscopy.

For the confocal microscopy experiments, an electrochemical compression cell similar to the one used for the electrocatalytic characterization (Figures 1a and S1) was employed. We note that the cell membrane was removed to accommodate the short focal length (1.7 mm) of the objective so that it could be positioned close to the cathode. Additionally, the cell was rotated 90° to accommodate the geometry of the confocal microscope. The choice and design of the electrochemical cell are further discussed in the Supporting Information. The DHPDS dye (100 μM) was dissolved in the electrolyte, and the electrolyte was replaced between every experiment to ensure that the initial conditions were standardized to keep the flux of hydroxide ions constant between experiments. The electrode was stable between experiments with minimal changes in the potential of the working electrode after 5 min (Figure S4). For each current density that was tested, a series of images were taken 3 μm apart in the z-direction (perpendicular to the electrode surface). Figure 3 shows two-dimensional (x, y) maps of solution pH obtained from a single location on the cathode surface at varying distances from the electrode surface (within a column) and at different current densities (along a row). The color scale in each map from blue to yellow denotes the local solution pH from pH = 7−10. The complete set of pH images

are shown in Figures S5−S10, and each set of images took approximately 30 min to collect.

In the first column of Figure 3, at 0 mA/cm^2, the solution pH is uniform throughout the z-direction. The second row of pH maps at 0 μm defines the surface of the electrode; as the electrode is not flat, the highest point of the electrode in the image area was chosen as the 0 μm height. Black regions in the pH map indicate areas where no fluorescence was observed and therefore no electrolyte was present. The bottom row of pH maps in Figure 3 shows the solution pH within a trench in the microporous layer. As the current density increases from left to right along a row, the local solution pH increases both within the trench of the microporous layer and above the electrode surface. It is particularly interesting to note that the pH is not completely uniform over the electrode surface, which can be most easily seen in the 0 and −15 μm height maps at a current density of −3.4 mA/cm^2. We are only able to observe this inhomogeneity at low current density where the pH gradient built up is not large. As the current density is further increased and all catalyst particles become electrochemically active, we are no longer able to disentangle the pH gradient creation from individual locations along the catalyst. This effect was repeatedly observed at multiple locations across the electrode surface, as shown in Figure S11. We observe much smaller local variations at −1.6 mA/cm^2 because the applied bias is smaller.

We can use pH as a proxy for the total current density, as each electron catalyzing either the HER or the CO_2 reduction reaction corresponds to the creation of one hydroxide ion in the electrolyte. Hence, higher pH regions are indicative of higher activity. As the current density was further increased, the fluorescent signal from the dye eventually saturates. To confirm that only electrochemically active areas of the electrode were responsible for locally increasing the solution pH, a map was obtained 9 μm above the electrode surface over a region that was only partially covered with Cu (Figure S12).
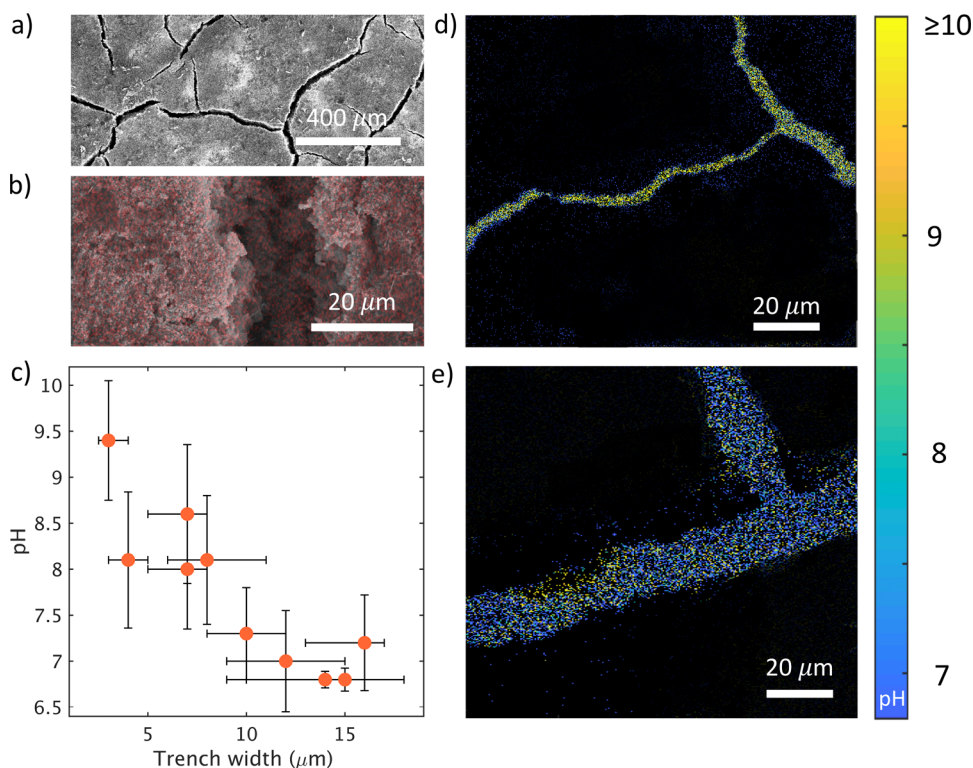
Figure 4. Influence of physical confinement on CO_2 reduction performance. (a) Low-magnification SEM image of a Cu gas diffusion electrode. (b) High-magnification SEM image of a Cu gas diffusion electrode with an overlay of the Cu signal obtained from an EDS map; red shading indicates Cu covered regions. (c) Measured pH as a function of trench width. The orange data points denote the average trench width. The error bars in the abscissa axis indicate the variation in trench width with the smallest and largest end points denoting the thinnest and widest points along the trench, respectively. The error bars in the ordinate axis represent the standard deviation of pH values within the trench. (d, e) pH maps obtained from two representative trenches with different widths located at different regions on the electrode at a distance of 8 μm below the electrode surface while operating at a current density of −3.4 mA/cm^2.

The electrolyte flowed left to right across the electrode, and the current density was set at −14.7 mA/cm^2. As shown in Figure S12a, the left-hand side of the map has a pH ∼7, which was obtained above a region of the catalyst without Cu, while the right-hand side of the map has a pH ∼9, which was taken from above a region coated in Cu. It is clear from this map that regions of locally high pH only occur near regions of the electrode where hydroxide ions are being created via electrocatalysis. In addition, we measured the pH under the same conditions as the back edge of the electrolyte (Figure S12b).

When the average pH at the surface of the electrode is below pH 9.5 ($J < −14.7$ mA/cm^2, or applied potentials less negative than −0.7 V vs RHE), the electrode mostly produces C_1 products and H_2. In contrast, many C_2 products were observed when the solution pH at the surface of the electrode was above pH 10 ($J > −28.0$ mA/cm^2, or at −1.0 V vs RHE). Potentials greater than −0.9 V vs RHE are required to produce these higher current densities and C_2 products, but the local pH also plays a role in suppressing the HER and promoting CO_2 reduction.[17,39] The activity of CO_2 reduction is independent, whereas the HER activity is greatly dependent on the hydroxide ion concentration.[17] For CO reduction on Cu, locally high pH conditions reduce the free energy required for important steps along the reaction pathway to yield C_2 products such as ethanol.[16] Areas of locally high pH may also reduce the free energy for CO_2 reduction pathways. Thus, our results indicate that a highly alkaline local pH increases the

selectivity toward C_2 products while decreasing the selectivity toward the HER.

Finally, we explore the local pH within trenches in the microporous layer, as shown in Figure 4. The trenches are randomly distributed throughout the electrode and have an average width of 18.8 ± 8 μm (Figure 4a). Figure 4b shows a higher-magnification SEM image of a crack, with an overlay of an energy-dispersive spectroscopy (EDS) map indicating regions that contain Cu (red shading). Figures S13 and S14 show more EDS maps of Cu, F, and C from different trenches. From these data, we found that Cu is coated not only on top of the microporous layer but also at the bottom and on the sides of the trenches, suggesting that CO_2 reduction can be performed within these confined regions of the electrode. These trenches within the microporous layer offer an interesting opportunity for studying the influence of physical confinement on the CO_2 reduction process in a GDE device. Accordingly, we employed our pH mapping techniques to these regions of the electrode to see how the reduced dimensions of the device influence the local solution pH near the active Cu electrocatalyst. At a current density of −3.4 mA/cm^2, we found that the solution pH within a narrow trench (∼3.2 μm wide) was pH 9.5. We emphasize that this local pH was much higher than the pH of 7.3 within a comparatively wider trench (∼16.2 μm wide). Interestingly, even at this relatively low current density (−3.4 mA/cm^2), the more confined electrochemically active region produces a higher local pH than more open regions, which serves to suppress the HER without substantially impeding CO_2 reduction.[47,48] We
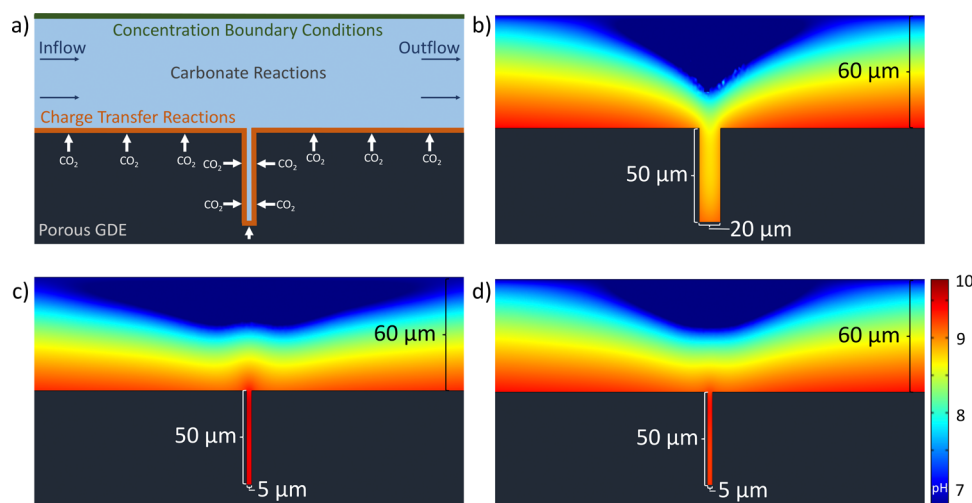
Figure 5. Simulations of local pH within and around trenches of various dimensions in the GDE. (a) Schematic of the model used for simulations indicating regions of CO_2 flux (white), current density (orange), concentration boundary conditions (green), and electrolyte flow (blue). pH map in the $x - z$ plane at a uniform current density of -3.4 mA/cm^2 for a trench with a depth of 50 μm and widths of (b) 20 μm and (d) 5 μm. (c) pH map in the $x - z$ plane for a trench [50 deep $\times$ 5 μm wide] with an average current density of -3.4 mA/cm^2, where the current density in the trench is twice as high as the current density on the surface. The CO_2 flux is constant through all surfaces, and boundary conditions are kept the same for all simulations. The pH scale bar applies to all pH profiles (b)−(d).

also note that the pH within a narrow trench is higher than the surrounding surface of the electrode (Figure S15). We proceeded to map to elucidate the trend of local pH vs. trench width, as shown in Figure 4c. While we find that the electrolyte flow is very small between the objective and the catalyst in our COMSOL flow model (Figure S16), we only measured the pH within trenches that were perpendicular to the electrolyte flow to ensure that the flow dynamics are as comparable as possible. We observed that as the trench width decreased, the local solution pH within the trench increased. This observation is consistent with prior electrochemical studies[17,47] and has important implications for the design of more active GDEs capable of performing selective CO_2 reduction at lower overpotentials with improved energy efficiency.

We additionally confirm the experimentally measured pH within the trenches for various widths and current densities by simulating the solution pH using the charge transfer and bulk reactions in a two-dimensional COMSOL model (Figure 5).[49] For the model (Figure 5a), we assumed a constant flux of CO_2 of 1 μmol/(cm^2 s) through the planar electrode surface, the trench walls, and trench bottom (see the SI for details). We used the experimental current density of -3.4 mA/cm^2 at the same boundaries because SEM and EDS images of our samples show that copper coats the surface, trench sidewalls, and trench bottom (see Figures S13 and S14). We assume a boundary layer thickness of 60 μm where a concentration boundary condition matching the concentration of CO_2-saturated 100 mM KHCO$_3$ electrolyte was applied. The electrolyte flow from left to right was also taken into consideration in the model. The appropriate flow velocity is determined with a three-dimensional COMSOL model of the flow in the electrochemical cell (Figure S16). For further discussion of the model setup, refer to the Supporting Information.

As we expected, the pH was increased close to the electrode surface and inside the trench due to charge transfer reactions locally creating hydroxide ions. The pH decreased further away from the electrode surface due to convection and diffusion within the bulk electrolyte. There was a dip in the pH profile above the trench because more CO_2 comes through the electrode at this point and acidifies the electrolyte close to the trench. Additionally, there is increased CO_2 flux here because CO_2 is able to diffuse not only through the bottom of the trench but also through the sidewalls. This feature was also observed experimentally, as shown in the pH map in Figure 3 for -3.4 mA/cm^2 at -15 μm and Figure S7. We note that the pH gradient is nearly symmetric above the crack because the electrolyte velocity is low. At higher current densities, we observed that pH increases in the trench and on the surface of the electrode as expected (Figure S17).

Comparing Figure 5b,d, it is clear that the pH is considerably lower in the wider trenches than the narrower trenches, which is in agreement with experimental results (Figure 4c). In Figure 5c, we simulated a trench with the same dimensions as the trench shown in Figure 5d. However, we modeled a nonuniform catalyst activity where the activity in the trench is twice as high as it is on the electrode surface, while maintaining the same average current density over the whole electrode. We observed that in this case, the pH within the trench is higher than the pH above the surface of the electrode, which we did not observe in experiment (see Figure S15). This discrepancy leads to the conclusion that the experimentally observed higher pH in narrow trenches cannot only be explained by the confinement of the trench, but must also be due to increased catalytic activity within the trench.

CONCLUSIONS

In conclusion, we have employed confocal fluorescence microscopy to elucidate how the *operando* local pH changes with current density as a function of distance above and below the surface of a Cu-based GDE. It is clear from the experimentally obtained pH maps that there are nonuniform hotspots of locally high pH across the catalyst even at relatively low overpotentials. Through experimental results confirmed by simulations, we show that the catalyst within narrow trenches

is more active than catalyst at the surface of the electrode. We also observed that the pH was higher in narrow trenches as opposed to wider trenches, and we confirmed this result with COMSOL simulations. Further work must be performed to understand why catalyst in narrow trenches performs better than catalyst in wider trenches, and this will be the subject of ongoing studies. Nevertheless, the ability to locally image the solution pH in three dimensions (x, y, and z) with micron spatial resolution is an important tool for understanding and identifying which part of the catalyst is most productive under real operating conditions. Our results have therefore demonstrated that the overpotential required to perform selective CO_2 reduction can be reduced within narrow trenches. We anticipate that this knowledge will help inform the design and construction of more efficient CO_2 reduction devices.

■ ASSOCIATED CONTENT

ⓈⒾ Supporting Information

The Supporting Information is available free of charge at https://pubs.acs.org/doi/10.1021/acs.jpcc.1c06265.

Materials; fabrication of copper electrodes; scanning electron microscopy characterization; energy-dispersive X-ray spectroscopy characterization; electrocatalytic CO_2 reduction reaction experiments for product analysis; electrocatalytic CO_2 reduction reaction experiments for pH imaging; choice of electrochemical cell; and COMSOL pH model (PDF)

■ AUTHOR INFORMATION

Corresponding Author

Harry A. Atwater − *Department of Applied Physics and Material Science, California Institute of Technology, Pasadena, California 91125, United States; Liquid Sunlight Alliance, California Institute of Technology, Pasadena, California 91125, United States;* ⓘ orcid.org/0000-0001-9435-0201; Email: haa@caltech.edu

Authors

Alex J. Welch − *Department of Applied Physics and Material Science, California Institute of Technology, Pasadena, California 91125, United States; Liquid Sunlight Alliance, California Institute of Technology, Pasadena, California 91125, United States;* ⓘ orcid.org/0000-0003-2132-9617

Aidan Q. Fenwick − *Department of Chemistry and Liquid Sunlight Alliance, California Institute of Technology, Pasadena, California 91125, United States*

Annette Böhme − *Department of Applied Physics and Material Science, California Institute of Technology, Pasadena, California 91125, United States; Liquid Sunlight Alliance, California Institute of Technology, Pasadena, California 91125, United States*

Hsiang-Yun Chen − *Department of Chemistry, California Institute of Technology, Pasadena, California 91125, United States;* ⓘ orcid.org/0000-0002-6461-1519

Ian Sullivan − *Liquid Sunlight Alliance, California Institute of Technology, Pasadena, California 91125, United States;* ⓘ orcid.org/0000-0003-0632-4607

Xueqian Li − *Department of Applied Physics and Material Science, California Institute of Technology, Pasadena, California 91125, United States; Liquid Sunlight Alliance,*
California Institute of Technology, Pasadena, California 91125, United States

Joseph S. DuChene − *Department of Chemistry, University of Massachusetts, Amherst, Massachusetts 01003, United States;* ⓘ orcid.org/0000-0002-7145-323X

Chengxiang Xiang − *Liquid Sunlight Alliance, California Institute of Technology, Pasadena, California 91125, United States;* ⓘ orcid.org/0000-0002-1698-6754

Complete contact information is available at:
https://pubs.acs.org/10.1021/acs.jpcc.1c06265

Notes

The authors declare no competing financial interest.

■ REFERENCES

(1) Hori, Y.; Kikuchi, K.; Suzuki, S. Production of CO and CH_4 in the Electrochemical Reduction of CO_2 at Metal Electrodes in Aqueous Hydrogencarbonate Solution. *Chem. Lett.* **1985**, *14*, 1695−1698.

(2) Kortlever, R.; Shen, J.; Schouten, K. J. P.; Calle-Vallejo, F.; Koper, M. T. M. Catalysts and Reaction Pathways for the Electrochemical Reduction of Carbon Dioxide. *J. Phys. Chem. Lett.* **2015**, *6*, 4073−4082.

(3) Bagger, A.; Ju, W.; Varela, A. S.; Strasser, P.; Rossmeisl, J. Electrochemical CO_2 Reduction: A Classification Problem. *ChemPhysChem* **2017**, *18*, 3266−3273.

(4) Kuhl, K.; Cave, E. R.; Abram, D. N.; Jaramillo, T. F. New Insights into the Electrochemical Reduction of Carbon Dioxide on Metallic Copper Surfaces. *Energy Environ. Sci.* **2012**, *5*, 7050−7059.

(5) Cave, E. R.; Montoya, J. H.; Kuhl, K. P.; Abram, D. N.; Hatsukade, T.; Shi, C.; Hahn, C.; Nørskov, J. K.; Jaramillo, T. F. Electrochemical CO_2 Reduction on Au Surfaces: Mechanistic Aspects Regarding the Formation of Major and Minor Products. *Phys. Chem. Chem. Phys.* **2017**, *19*, 15856−15863.

(6) Endrődi, B.; Bencsik, G.; Darvas, F.; Jones, R.; Rajeshwar, K.; Janáky, C. Continuous-Flow Electroreduction of Carbon Dioxide. *Prog. Energy Combust. Sci.* **2017**, *62*, 133−154.

(7) Bohlen, B.; Wastl, D.; Radomski, J.; Sieber, V.; Vieira, L. Electrochemical CO_2 Reduction to Formate on Indium Catalysts Prepared by Electrodeposition in Deep Eutectic Solvents. *Electrochem. Commun.* **2020**, *110*, No. 106597.

(8) Singh, M. R.; Kwon, Y.; Lum, Y.; Ager, J. W.; Bell, A. T. Hydrolysis of Electrolyte Cations Enhances the Electrochemical Reduction of CO_2 over Ag and Cu. *J. Am. Chem. Soc.* **2016**, *138*, 13006−13012.

(9) Jeanty, P.; Scherer, C.; Magori, E.; Wiesner-Fleischer, K.; Hinrichsen, O.; Fleischer, M. Upscaling and Continuous Operation of Electrochemical CO_2 to CO Conversion in Aqueous Solutions on Silver Gas Diffusion Electrodes. *J. CO2 Util.* **2018**, *24*, 454−462.

(10) Weekes, D. M.; Salvatore, D. A.; Reyes, A.; Huang, A.; Berlinguette, C. P. Electrolytic CO2 Reduction in a Flow Cell. *Acc. Chem. Res.* **2018**, *51*, 910−918.

(11) Rabinowitz, J. A.; Kanan, M. W. The Future of Low-Temperature Carbon Dioxide Electrolysis Depends on Solving One Basic Problem. *Nat. Commun.* **2020**, *11*, No. 5231.

(12) Kim, B.; Hillman, F.; Ariyoshi, M.; Fujikawa, S.; Kenis, P. J. A. Effects of Composition of the Microporous Layer and the Substrate on Performance in the Electrochemical Reduction of CO_2 to CO. *J. Power Sources* **2016**, *312*, 192−198.

(13) Davis, S. J.; Lewis, N. S.; Shaner, M.; Aggarwal, S.; Arent, D.; Azevedo, I. L.; Benson, S. M.; Bradley, T.; Brouwer, J.; Chiang, Y.; et al. Net-Zero Emissions Energy Systems. *Science* **2018**, *360*, No. eaas9793.

(14) Birdja, Y. Y.; Pérez-Gallent, E.; Figueiredo, M. C.; Göttle, A. J.; Calle-Vallejo, F.; Koper, M. T. M. Advances and Challenges in Understanding the Electrocatalytic Conversion of Carbon Dioxide to Fuels. *Nat. Energy* **2019**, *4*, 732−745.

(15) Leenheer, A. J.; Atwater, H. A. Imaging Water-Splitting Electrocatalysts with PH-Sensing Confocal Fluorescence Microscopy. *J. Electrochem. Soc.* **2012**, *159*, H752−H757.

(16) Liu, X.; Schlexer, P.; Xiao, J.; Ji, Y.; Wang, L.; Sandberg, R. B.; Tang, M.; Brown, K. S.; Peng, H.; Ringe, S.; et al. pH Effects on the Electrochemical Reduction of CO_2 towards C2 Products on Stepped Copper. *Nat. Commun.* **2019**, *10*, No. 32.

(17) Hall, A. S.; Yoon, Y.; Wuttig, A.; Surendranath, Y. Mesostructure-Induced Selectivity in CO_2 Reduction Catalysis. *J. Am. Chem. Soc.* **2015**, *137*, 14834−14837.

(18) Zhang, Z.; Melo, L.; Jansonius, R. P.; Habizadeh, F.; Grant, E. R.; Berlinguette, C. P. PH Matters When Reducing CO_2 in an Electrochemical Flow Cell. *ACS Energy Lett.* **2020**, *5*, 3101−3107.

(19) Higgins, D.; Hahn, C.; Chengxiang, X.; Jaramillo, T. F.; Weber, A. Z. Gas-Diffusion Electrodes for Carbon Dioxide Reduction: A New Paradigm. *ACS Energy Lett.* **2019**, *4*, 317−324.

(20) Inaba, M.; Jensen, A. W.; Sievers, G. W.; Escudero-Escribano, M.; Zana, A.; Arenz, M. Benchmarking High Surface Area Electrocatalysts in a Gas Diffusion Electrode: Measurement of Oxygen Reduction Activities under Realistic Conditions. *Energy Environ. Sci.* **2018**, *11*, 988−994.

(21) Nitopi, S.; Bertheussen, E.; Scott, S. B.; Liu, X.; Engstfeld, A. K.; Horch, S.; Seger, B.; Stephens, I. E. L.; Chan, K.; Hahn, C.; et al. Progress and Perspectives of Electrochemical CO_2 Reduction on Copper in Aqueous Electrolyte. *Chem. Rev.* **2019**, *119*, 7610−7672.

(22) Singh, M. R.; Clark, E. L.; Bell, A. T. Effects of Electrolyte, Catalyst, and Membrane Composition and Operating Conditions on the Performance of Solar-Driven Electrochemical Reduction of Carbon Dioxide. *Phys. Chem. Chem. Phys.* **2015**, *17*, 18924−18936.

(23) Weng, L.-C.; Bell, A. T.; Weber, A. Z. Modeling Gas-Diffusion Electrodes for CO_2 Reduction. *Phys. Chem. Chem. Phys.* **2018**, *20*, 16973−16984.

(24) García de Arquer, F. P.; Dinh, C. T.; Ozden, A.; Wicks, J.; McCallum, C.; Kirmani, A. R.; Nam, D. H.; Gabardo, C.; Seifitokaldani, A.; Wang, X.; et al. CO_2 Electrolysis to Multicarbon Products at Activities Greater than 1 A Cm^{-2}. *Science* **2020**, *367*, 661−666.

(25) Dinh, C.; Burdyny, T.; Kibria, G.; Seifitokaldani, A.; Gabardo, C. M.; Arquer, F. P. G.; De; Kiani, A.; Edwards, J. P.; Luna, P.; De; Bushuyev, O. S.; et al. CO_2 Electroreduction to Ethylene via Hydroxide-Mediated Copper Catalysis at an Abrupt Interface. *Science* **2018**, *360*, 783−787.

(26) Wang, L.; Nitopi, S. A.; Bertheussen, E.; Orazov, M.; Morales-Guio, C. G.; Liu, X.; Higgins, D. C.; Chan, K.; Nørskov, J. K.; Hahn, C.; Jaramillo, T. F. Electrochemical Carbon Monoxide Reduction on Polycrystalline Copper: Effects of Potential, Pressure, and PH on Selectivity toward Multicarbon and Oxygenated Products. *ACS Catal.* **2018**, *8*, 7445−7454.

(27) Nesbitt, N.; Smith, W. Water Activity Regulates CO_2 Reduction in Gas-Diffusion Electrodes. *ChemRxiv* 2021.

(28) Suter, S.; Haussener, S. Optimizing Mesostructured Silver Catalysts for Selective Carbon Dioxide Conversion into Fuels. *Energy Environ. Sci.* **2019**, *12*, 1668−1678.

(29) Monteiro, M. C. O.; Koper, M. T. M. Measuring Local PH in Electrochemistry. *Curr. Opin. Electrochem.* **2021**, *25*, No. 100649.

(30) Rudd, N. C.; Cannan, S.; Bitziou, E.; Ciani, I.; Whitworth, A.; Unwin, P. R. Fluorescence Confocal Laser Scanning Microscopy as a Probe of PH Gradients in Electrode Reactions and Surface Activity Nicola. *Anal. Chem.* **2005**, *77*, 6205−6217.

(31) Bouffier, L.; Doneux, T. Coupling Electrochemistry with in Situ Fluorescence (Confocal) Microscopy. *Curr. Opin. Electrochem.* **2017**, *6*, 31−37.

(32) Pande, N.; Chandrasekar, S. K.; Lohse, D.; Mul, G.; Wood, J. A.; Mei, B. T.; Krug, D. Electrochemically Induced PH Change: Time-Resolved Confocal Fluorescence Microscopy Measurements and Comparison with Numerical Model. *J. Phys. Chem. Lett.* **2020**, *11*, 7042−7048.

(33) Vitt, J. E.; Engstrom, R. C. Imaging of Oxygen Evolution and Oxide Formation Using Quinine Fluorescence. *Anal. Chem.* **1997**, *69*, 1070−1076.

(34) Bowyer, W. J.; Xie, J.; Engstrom, R. C. Fluorescence Imaging of the Heterogeneous Reduction of Oxygen. *Anal. Chem.* **1996**, *68*, 2005−2009.

(35) Nesbitt, N.; Smith, W. A. Operando Topography and Mechanical Property Mappinig of CO_2 Reduction Gas-Diffusion Electrodes Operating at High Currrent Densities. *J. Electrochem. Soc.* **2021**, *168*, No. 044505.

(36) Botz, A.; Clausmeyer, J.; Öhl, D.; Tarnev, T.; Franzen, D.; Turek, T.; Schuhmann, W. Local Activities of Hydroxide and Water Determine the Operation of Silver-Based Oxygen Depolarized Cathodes. *Angew. Chem., Int. Ed.* **2018**, *57*, 12285−12289.

(37) Dieckhöfer, S.; Öhl, D.; Junqueira, J. R. C.; Quast, T.; Turek, T.; Schuhmann, W. Probing the Local Reaction Environment During High Turnover Carbon Dioxide Reduction with Ag-Based Gas Diffusion Electrodes. *Chem. - Eur. J.* **2021**, *27*, 5906−5912.

(38) Lu, X.; Zhu, C.; Wu, Z.; Xuan, J.; Francisco, J. S.; Wang, H. In Situ Observation of the PH Gradient near the Gas Diffusion Electrode of CO_2 Reduction in Alkaline Electrolyte. *J. Am. Chem. Soc.* **2020**, *142*, 15438−15444.

(39) Yang, K.; Kas, R.; Smith, W. A. In Situ Infrared Spectroscopy Reveals Persistent Alkalinity near Electrode Surfaces during CO_2 Electroreduction. *J. Am. Chem. Soc.* **2019**, *141*, 15891−15900.

(40) Nitopi, S.; Bertheussen, E.; Scott, S. B.; Liu, X.; Engstfeld, A. K.; Horch, S.; Seger, B.; Stephens, I. E. L.; Chan, K.; Hahn, C.; et al. Progress and Perspectives of Electrochemical CO2 Reduction on Copper in Aqueous Electrolyte. *Chem. Rev.* **2019**, *119*, 7610−7672.

(41) Wang, Y.; Shen, H.; Livi, K. J. T.; Raciti, D.; Zong, H.; Gregg, J.; Onadeko, M.; Wan, Y.; Watson, A.; Wang, C. Copper Nanocubes for CO_2 Reduction in Gas Diffusion Electrodes. *Nano Lett.* **2019**, *19*, 8461−8468.

(42) Nguyen, T. N.; Dinh, C. T. Gas Diffusion Electrode Design for Electrochemical Carbon Dioxide Reduction. *Chem. Soc. Rev.* **2020**, *49*, 7488−7504.

(43) Ripatti, D. S.; Veltman, T. R.; Kanan, M. W. Carbon Monoxide Gas Diffusion Electrolysis That Produces Concentrated C2 Products with High Single-Pass Conversion. *Joule* **2019**, *3*, 240−256.

(44) Welch, A. J.; Dunn, E.; Duchene, J. S.; Atwater, H. A. Bicarbonate or Carbonate Processes for Coupling Carbon Dioxide Capture and Electrochemical Conversion. *ACS Energy Lett.* **2020**, *5*, 940−945.

(45) Hakonen, A.; Hulth, S. A High-Performance Fluorosensor for PH Measurements between 6 and 9. *Talanta* **2010**, *80*, 1964−1969.

(46) Hori, Y. Electrochemical CO 2 Reduction on Metal Electrodes. *Mod. Aspects Electrochem.* **2008**, *42*, 89−189.

(47) Welch, A. J.; Duchene, J. S.; Tagliabue, G.; Davoyan, A.; Cheng, W. H.; Atwater, H. A. Nanoporous Gold as a Highly Selective and Active Carbon Dioxide Reduction Catalyst. *ACS Appl. Energy Mater.* **2019**, *2*, 164−170.

(48) Hall, A. S.; Yoon, Y.; Wuttig, A.; Surendranath, Y. Mesostructure-Induced Selectivity in CO_2 Reduction Catalysis. *J. Am. Chem. Soc.* **2015**, *137*, 14834−14837.

(49) Schulz, K. G.; Riebesell, U.; Rost, B.; Thoms, S.; Zeebe, R. E. Determination of the Rate Constants for the Carbon Dioxide to Bicarbonate Inter-Conversion in PH-Buffered Seawater Systems. *Mar. Geochem.* **2006**, *100*, 53−65.